Theoretical and experimental analysis of a floating flexible circular disk

S. Michele[a,c], S. Zheng[b,c], A.G.L. Borthwick[c], D.M. Greaves[c]

[a] Department of Civil Engineering and Computer Science, University of Rome Tor Vergata, Rome, Italy

[b] Ocean College, Zhejiang University, Zhoushan 316021, Zhejiang, China

[c] School of Engineering, Computing and Mathematics, University of Plymouth, UK

michele@ing.uniroma2.it

Introduction

This paper describes results from physical model tests undertaken in the COAST laboratory at the University of Plymouth. Response amplitude operators (RAOs) of a floating flexible circular disk are determined for incident monochromatic and irregular wave trains. Free-surface displacements are measured, and the plate motion recorded using a QUALISYS® motion tracking system. Different basin depths, plate thicknesses and wave amplitudes are considered. We present synchronous and subharmonic nonlinear responses for monochromatic waves, and displacement spectra for irregular waves. The measured wave hydrodynamics and disk hydroelastic responses match theoretical predictions.

Experimental set-up

The COAST Ocean basin is of length $L = 35$ m and width $B = 15.5$ m, and has a movable floor that accommodates an operating depth of up to $h = 3$ m. Water waves are generated by 24 individually controlled, hinged-flap, wave-absorbing paddles. Figures 1(a) - 1(b) show a perspective view of the model plate within the Ocean basin. The origin of the coordinate system is located at the initial disk centre position, x is the horizontal axis parallel to the major basin length, y is parallel to the wavemakers, and z points vertically upwards from still water level. The elastic disk of radius $R = 0.75$ m was fabricated from expanded polyvinyl chloride (PVC) FOREX®. Two circular plates of thickness $h_p = [3; 10]$ mm were tested in the experiments, for which we have $h_p \ll R$, and so our theoretical model is based on the thin plate approximation. Plate density ρ_p and Young's modulus E were evaluated experimentally because of uncertainty in the values specified by the supplier. For the 3 mm thickness plate we found $\rho_p = 489.64$ kg m^{-3} and $E = 854$ MPa, whereas for the 10 mm thickness plate we obtained $\rho_p = 463.87$ kg m^{-3} and $E = 508$ MPa. To prevent second-order plate drift, we added four horizontal moorings, each of length 3 m, connected by four vertical beams fixed to the basin gantries. The vertical beams are located at 45^o with respect to the incident wave direction, permitting symmetric response with respect to the horizontal axis x. Each mooring was fitted with a spring at its end, the spring having small stiffness ~ 8.73 N m^{-1} to avoid impulsive forces and large vertical reactions that are not taken into account in the theoretical model. In the experiments, we fixed a waterproof black neoprene foam barrier around the edge of the plate to avoid greenwater flooding which was not included in our mathematical model. Free-surface elevation time series were recorded using four wave gauges. The gauge locations are Gauge 1=[2.32;0] m, Gauge 2=[0;2.245] m, Gauge 3=[-2.71;0] m and Gauge 4=[5.522;0] m. Measurements were also collected in the wave basin in the absence of the plate and support structures. With the plate present, its response amplitude operator (RAO) was then determined. Plate movement was recorded by a motion tracking device developed by QUALISYS®. The movement measurement system comprised six infrared cameras that captured the three-dimensional positions of markers. The plate motion was excited by incident waves whose direction was parallel to the x-axis in order to produce a symmetric response by the disk. A total of 29 markers were fixed to the disk covering half its surface $y \geq 0$. The markers were distributed radially in accordance with the theory based on radial and circular eigenfrequencies. Figure 1(c) represents the location of the 29 markers. For brevity, in the subsequent analyses, we present the oscillations recorded only by markers 0 (located at the origin), 22, 25, and 28 (located close to the neoprene barrier). The coordinates of the markers are Marker 0=[0;0] m, Marker 22=[0.685;0] m, Marker 25=[0;0.685] m and Marker 28=[-0.685;0] m.

Tests summary: regular and irregular waves

Tests were carried out separately on two elastic disks of different thicknesses h_p in regular monochromatic waves. Data were collected for different wave frequencies in the range $f \in [0.4; 1.9]$ Hz with frequency increment $\Delta f = 0.05$ Hz. Two basin depths were considered, $h = [1.5; 3]$ m. A constant wave amplitude

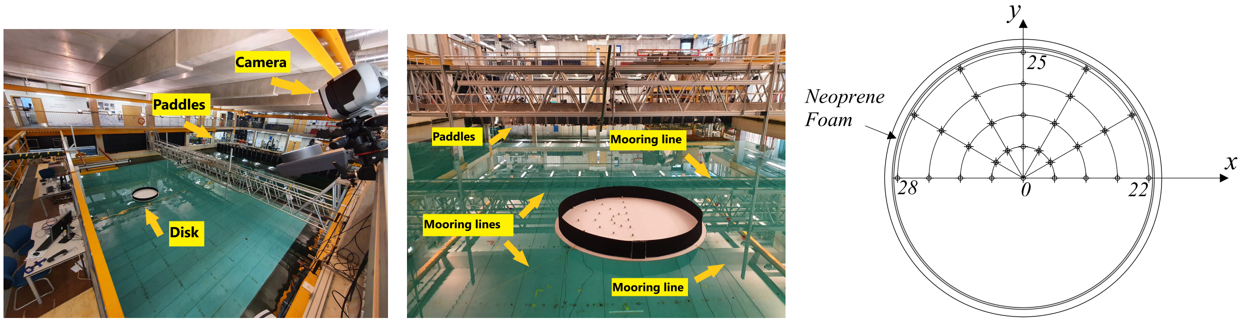

Figure 1: (a) View of the experimental set-up. One of the six cameras used for tracking motion is visible at the top-right of the picture. (b) View of elastic disk, markers, and mooring lines connected to the gantries. (c) Plan view of disk, neoprene foam barrier, and marker locations.

was selected, $A = 0.03$ m. In the smaller depth case, $h = 1.5$ m, measurements were recorded for a reduced wave amplitude $A = 0.02$ m in order to investigate possible nonlinear responses that were not proportional to A. Amplitude and basin depths for Case 1, Case 2 and Case 3 were respectively $A = [3; 3; 2]$ cm, and $h = [1.5; 3; 1.5]$ m. In the second series of tests, irregular waves were defined by the JONSWAP energy spectrum S_ζ. The basin depth was fixed at $h = 3$ m and significant wave height $H_s = 0.04$ m to avoid possible overtopping. Five values of peak period $T_p = [0.8; 0.9; 1.0; 1.1; 1.2]$ s were considered for each disk to analyse the effects of plate flexural rigidity and wave peak period on the plate response spectrum.

Mathematical model of the response of a disk to regular and irregular waves

Following [1] we define W as the vertical displacement of the disk above still water level and Φ as a complex velocity potential that satisfies Laplace's equation in the fluid domain. The system is forced by monochromatic incident waves of frequency ω, and so we introduce the following harmonic expansion $\{\Phi, W\} = \mathrm{Re}\left\{(\phi, w)e^{-\mathrm{i}\omega t}\right\}$ where ϕ is the scalar velocity potential, i is the imaginary unit, and t is time. Here, the plate undergoes symmetrical motion, oscillating through a combination of axisymmetric modes. Hence, $w = \zeta_h w_h + \zeta_p w_p + \sum_{m=0}^{\infty}\sum_{n=0}^{\infty}\zeta_{mn}w_{mn}$, where the first two terms represent heave and pitching, the series denote elastic bending modes, and ζ_α denotes the complex amplitude of each modal shape w_α. Let (r, θ) be radial and angular coordinates with $\theta = 0$ corresponding with the x axis and θ positive counter-clockwise. Heave and pitch modal shapes are $w_h = 1, w_p = r\cos\theta$, whereas the elastic dry modes are given by

$$w_{mn} = \cos n\theta \left[J_n\left(\frac{\lambda_{mn}r}{R}\right) - I_n\left(\frac{\lambda_{mn}r}{R}\right)T_{mn}\right], \quad T_{mn} = \left.\frac{J_n''\left(\frac{\lambda_{mn}r}{R}\right) - \frac{n^2\nu}{R^2}J_n\left(\frac{\lambda_{mn}r}{R}\right) + \frac{\nu}{R}J_n'\left(\frac{\lambda_{mn}r}{R}\right)}{I_n''\left(\frac{\lambda_{mn}r}{R}\right) - \frac{n^2\nu}{R^2}I_n\left(\frac{\lambda_{mn}r}{R}\right) + \frac{\nu}{R}I_n'\left(\frac{\lambda_{mn}r}{R}\right)}\right|_{r=R},$$

$n = 0, 1, .., m = 0, 1, ...,$ J_n and I_n are the Bessel function and modified Bessel function of order n, primes indicate the derivative with respect to the radial coordinate r, $\lambda_{mn}^4 = \rho_h h_p R^4 \omega_{mn}^2/D$ is the eigenvalue, and ω_{mn} is the eigenfrequency. We decompose ϕ into diffraction and radiation components, i.e. $\phi = \phi_D + \zeta_h\phi_h + \zeta_p\phi_p + \sum_{m=0}^{\infty}\sum_{n=0}^{\infty}\zeta_{mn}\phi_{mn}, \quad \phi_D = \phi_I + \phi_S$, where the incident wave potential is

$$\phi_I = -\frac{\mathrm{i}Ag}{\omega}\sum_{n=0}^{\infty}\epsilon_n \mathrm{i}^n J_n(k_0 r)\frac{\cosh k_0(h+z)}{\cosh k_0 h}\cos n\theta, \quad \text{in } \Omega_e,$$

the wavenumber k_0 is the real root of the dispersion relation $\omega^2 = gk_0\tanh(k_0 h)$, g is the acceleration due to gravity, ϕ_S is the scattering potential, ϕ_D is the diffraction potential, ϕ_h is the heaving radiation potential, ϕ_p is the pitching radiation potential, and ϕ_{mn} is the radiation potential related to the mn-th elastic mode.

Velocity potentials and plate motion

The general solution for the diffraction potential beyond the disk where $r > R$ is

$$\phi_D^{(e)} = -\frac{\mathrm{i}Ag}{\omega}\sum_{n=0}^{\infty}\cos n\theta\left\{\frac{\cosh k_0(h+z)}{\cosh k_0 h}\left[\epsilon_n \mathrm{i}^n J_n(k_0 r) + \frac{\mathcal{A}_{0n}^D H_n^{(1)}(k_0 r)}{H_n^{(1)\prime}(k_0 r)\Big|_{r=R}}\right] + \sum_{l=1}^{\infty}\frac{\mathcal{A}_{ln}^D K_n(\overline{k}_l r)\cos\overline{k}_l(h+z)}{K_n'(\overline{k}_l r)\big|_{r=R}\cos\overline{k}_l h}\right\},$$

where $\overline{k_l}$ denotes the roots of the dispersion relation related to the evanescent components $\omega^2 = -g\overline{k_l}\tan\overline{k_l}h$, $H_n^{(1)}$ is the Hankel function of first kind and order n, K_n is the modified Bessel function of second kind and order n, and $\mathcal{A}_{ln}$ are unknown complex constants. Similarly, the solution for the diffraction potential in the fluid domain below the circular plate is given by

$$\phi_D^{(i)} = -\frac{\mathrm{i}Ag}{\omega}\sum_{n=0}^{\infty}\cos n\theta\left\{\mathcal{B}_{0n}^{D}\left(\frac{r}{R}\right)^n + \sum_{l=1}^{\infty}\mathcal{B}_{ln}^{D}\frac{I_n(\mu_l r)\cos\mu_l(h+z)}{I_n'(\mu_l r)|_{r=R}\cos\mu_l h}\right\},\ \mu_l = \frac{l\pi}{h},$$

where $\mathcal{B}_{ln}^{D}$ are unknown coefficients which are determined numerically as by [1]. The general solution in the region $r > R$ for each radiation velocity potential α is

$$\phi_\alpha^{(e)} = \sum_{n=0}^{\infty}\cos n\theta\left\{\mathcal{A}_{0n}^{\alpha}\frac{H_n^{(1)}(k_0 r)\cosh k_0(h+z)}{H_n^{(1)\prime}(k_0 r)\Big|_{r=R}\cosh k_0 h} + \sum_{l=1}^{\infty}\mathcal{A}_{ln}^{\alpha}\frac{K_n(\overline{k_l}r)\cos\overline{k_l}(h+z)}{K_n'(\overline{k_l}r)\big|_{r=R}\cos\overline{k_l}h}\right\},$$

where the value of the subscript α refers to heave, pitch, or mn-th bending elastic mode. The radiation potential solution in the region below the plate where $r < R$ is given by the homogeneous part $\phi_{\alpha h}^{(i)}$ in addition to a particular solution that accounts for the plate vibration. The homogeneous component is

$$\phi_{\alpha h}^{(i)} = \sum_{n=0}^{\infty}\cos n\theta\left\{\mathcal{B}_{0n}^{\alpha}\left(\frac{r}{R}\right)^n + \sum_{l=1}^{\infty}\mathcal{B}_{ln}^{\alpha}\frac{I_n(\mu_l r)\cos\mu_l(h+z)}{I_n'(\mu_l r)|_{r=R}\cos\mu_l h}\right\}, \tag{1}$$

whereas the structure of each particular solution is independent of the others. Applying separation of variables, the particular solution for the rigid heave and pitching modes is

$$\tilde{\phi}_h = -\frac{\mathrm{i}\omega}{2h}\left[z^2 + 2hz - \frac{r^2}{2}\right],\ \tilde{\phi}_p = -\frac{\mathrm{i}\omega r\cos\theta}{8h}\left[4z^2 + 8hz - r^2\right], \tag{2}$$

and the particular solution for each bending elastic mode is

$$\tilde{\phi}_{mn} = -\mathrm{i}\omega R\frac{\cos n\theta}{\lambda_{mn}}\left\{\frac{\cosh\frac{\lambda_{mn}(h+z)}{R}J_n\left(\frac{\lambda_{mn}r}{R}\right)}{\sinh\frac{\lambda_{mn}h}{R}} + \frac{\cos\frac{\lambda_{mn}(h+z)}{R}I_n\left(\frac{\lambda_{mn}r}{R}\right)}{\sin\frac{\lambda_{mn}h}{R}}T_{mn}\right\},\quad n = 0, 1, ... \tag{3}$$

As before, the unknowns $\mathcal{A}_{ln}^{\alpha}$, $\mathcal{B}_{ln}^{\alpha}$ have to be determined numerically. The modal amplitudes are obtained from the equation of motion of the disk. Assuming that the mooring system and neoprene foam rigidity have negligible effects, the dynamic equation can be written as $D\nabla^4 W + \rho_p h_p W_{tt} + \rho g W + \rho\Phi_t = 0$, where $D = Eh_p^3/12(1-\nu^2)$ is the flexural rigidity, E is the Young's modulus of the plate material, $\nu = 0.3$ is Poisson's ratio, ∇^4 denotes the biharmonic operator in cylindrical-polar coordinates, ρ is the fluid density, and the subscripts denote differentiation with respect to the relevant variable. By using the dry mode decomposition [2] we obtain a system expressed in terms of complex modal amplitudes ζ_h, ζ_p and ζ_{mn}. The resulting linear system is then written in the matrix form $\mathbf{M}\{\zeta\} = \{F\}$ where $\mathbf{M}$ is the coefficient matrix, $\{F\}$ is the exciting force vector, and $\{\zeta\}$ is a vector of unknown modal amplitudes. Once the complex amplitudes are evaluated, the marker displacement is given by substituting the marker coordinates into the expansion for w. Noting that the theoretical model is based on a linear assumption, the time-dependent oscillation of the flexible disk in irregular waves can be written as $W = \sum_{n=1}^{\infty}\sqrt{2S_\zeta(\omega_n)\Delta\omega}\,\mathrm{RAO}(\omega_n, r, \theta)\cos(\omega_n t + \delta_n)$, where ω_n is the nth component of the discretised spectrum, $\Delta\omega$ is the frequency interval, δ_n is a random phase related to ω_n, and RAO is the Response Amplitude Operator for the plate defined as $\mathrm{RAO}(\omega_n, r, \theta) = |W|/A$. The theoretical response spectrum is consequently given by $S_w = S_\zeta \times \mathrm{RAO}^2$.

Synchronous linear response to monochromatic waves

The plate response at leading order is synchronous with incident wave frequency. Let us consider Case 1, Figure 2(a) presents the response amplitude operator versus wave frequency for markers 0, 22, 25, and 28, and plate thickness $h_p = 10$ mm. Bearing in mind the limitations of the theoretical model, good agreement

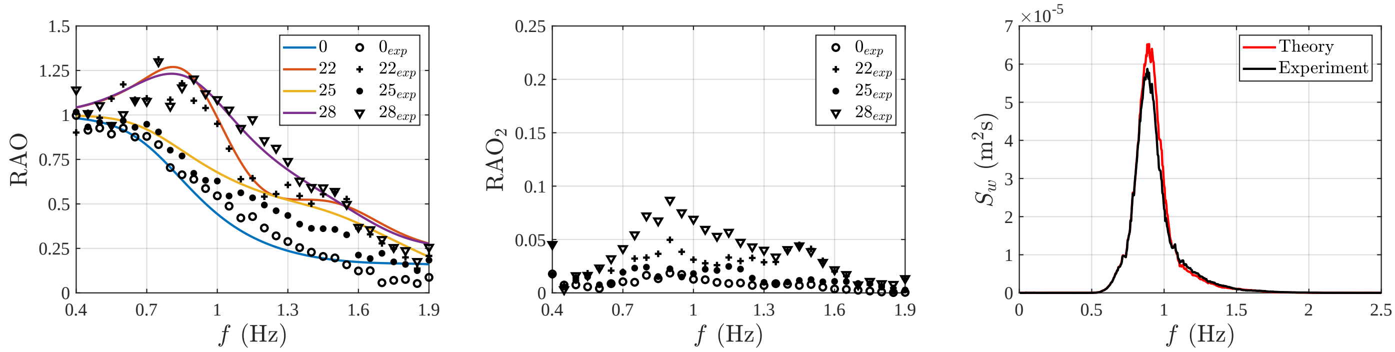

Figure 2: (a) Response amplitude operator versus frequency at marker locations 0, 22, 25 and 28 for Case 1, and $h_p = 10$ mm. Solid lines depict the analytical solution whereas symbols represent the experimental results. (b) Normalised second harmonic response contributions versus wave frequency at marker locations 0, 22, 25 and 28 for Case 1 and $h_p = 10$ mm. (c) Vertical displacement spectra for $H_s = 0.04$ m, $T_p = 1.2$ s and $h_p = 10$ mm at Marker 28. The red line corresponds to theory, and the black line is obtained from the measured displacement time series.

is achieved between the theoretical RAO curve and the experimental RAO_{exp} values. We remark that the theoretical model over-predicts the plate response, especially when higher bending mode resonance occurs. This occurs primarily because hydrodynamic damping and viscoelastic behaviour of the disk are neglected. Even so, the mathematical model properly reproduces the experimental rigid modes and first bending mode resonance locations; this is due to the larger added mass arising from the plate motion, which reduces damping. Additional experimental results will be shown at the workshop but we anticipate that good agreement is found in the other case studies.

Second and third harmonic response

By following a perturbation approach, quadratic and cubic nonlinear terms are included in the boundary conditions, leading to contributions of order $O(\epsilon)$ or smaller [3]. In the present experiments $\epsilon \ll 1$, and so we expect the higher harmonic responses to be less pronounced than the linear synchronous behaviour. Herein, the response amplitude operators of the second and third harmonics are denoted by RAO_2 and RAO_3. Figure 2(b) displays experimental second-harmonic RAO according to incident wave frequency for Case 1 where $h_p = 10$ mm, at marker locations 0, 22, 25, and 28. RAO_2 is significantly smaller than the linear response in Figure 2(a). This is because subharmonics are at most $O(\epsilon)$ order effects and the wave steepness is very small in this case. Even so, the second harmonic component can be important as evidenced by RAO_2 approaching ~ 0.1 for $f = 0.9$ Hz. This peak, recorded at marker 28, warrants further theoretical investigation through weakly nonlinear approaches. We believe the peak arises from the presence of several natural bending modes in the frequency range of interest where multi-resonance is possible. RAO_3 and further comparisons for the smaller plate thickness $h_p = 3$ mm will be shown at the workshop. In this case we found a stronger nonlinear response.

Response to irregular waves

We next examine disk response spectra obtained by analysing the measured vertical displacements of markers 0, 22, 25, and 28. Figure 2(c) compares the smoothed experimental and theoretical response spectra obtained at marker 28 for $h_p = 10$ mm and peak period $T_p = 1.2$ s. The theoretical model (red line) properly represents the experimental response (black line) in irregular waves. We anticipate that agreement is also found in the case of smaller plate thickness and other peak periods. These additional results will be shown at the workshop.

REFERENCES

[1] Michele, S., Zheng, S., and Greaves, D. M. 2022. *Wave energy extraction from a floating flexible circular plate. Ocean Eng. 245*, 110275.

[2] Newman, J. N. 1994. *Wave effects on deformable bodies. Appl. Ocean Res. 16*, 47–59.

[3] Mei, C. C., Stiassnie, M., and Yue, D. K.-P. 2005. *Theory and application of ocean surface waves.* World Scientific, Singapore.